Immune Tumor Microenvironment of HIV-Associated Lung Cancer Reveals Immunoregulatory Features

787

Syim Salahuddin, Ramsey Yusuf, Shruti Desai, Kishu Ranjan, Jianlei Gu, Lais Osmani, Insoo Kang, Hongyu Zhao, Yuval Kluger, Kurt Schalper, Brinda Emu

Yale University, New Haven, CT

Background
Lung cancer is the leading cause of cancer mortality among people with HIV (PWH), with increased incidence and poor outcomes.
Methods
We explored whether HIV-associated non-small cell lung cancers (NSCLC) harbor an immunoregulatory tumor microenvironment (TME) that limits tumor-specific responses. A tissue microarray was constructed with tumors from 18 PWH and 19 people without HIV (PWOH), matched for histological subtype, stage, year of diagnosis, age, sex and smoking status. imaging mass cytometry was employed with 40 immune cell markers for TME characterization. Linear mixed effects model, AI-based pageRank mathematical algorithm based on spectral graph theory, and neighborhood enrichment analysis were employed.
Results
NSCLC from PWH demonstrated differential distribution of tumor-infiltrating CD8+ T cell clusters defined by marker expression patterns, enriched for the expression of PD-1 and Lag-3, as well as activation and proliferation markers, compared to tumors from PWOH. Several clusters of T cells were significantly elevated in tumors from PWH, with the strikingly the finding of significant increased proportion of "Exhausted burned out CD8+ T cells" that have high levels of PD-1, Lag-3, Tbet and Ki67 (Fold change increase of 4.21 in PWH, p<0.0001). We also demonstrate higher expression of immunoregulatory molecules (PD-L1, PD-L2, B7-H3, B7-H4, IDO1 and VISTA), among tumor-associated macrophages, confirmed by the expansion of three unique TAM clusters comprising 58.8% of TAMs vs. 17.8% in tumors from PWH vs PWOH respectively (p<0.0001). An unsupervised and cell segmentation-independent signature associated using spectral graph theory methodology discriminated cells between HIV-associated and non-HIV tumors with 84.6% accuracy, with confirmation of the cell segmentation approach. Furthermore, we noted differences in spatial orientation of immune cells within the TME of PWH compared to PWOH, with evidence of increased Euclidean distance between each immune cell subtype (CD8 and CD4 T cells, and TAM) and CK+ tumor cells among PWH (p<0.0001 for each pair of cell types).

Table 1: Cohort Characteristics

	PWH-NSCLC N=18	PWOH-NSCLC N=19	P value
Median Age	54.1	57.2	0.22
Male Gender	14 (78%)	9 (47%)	0.06
Smoking Status			
Non-smoking	0	2 (11%)	0.49
Smoker History	18 (100%)	17 (89%)	
Year of Diagnosis			
1999-2004	4 (22%)	6 (32%)	
2005-2010	8 (44%)	6 (32%)	0.70
2011-2016	6 (33%)	7 (37%)	
Histology			
Adenocarcinoma	8 (44%)	10 (53%)	
Squamous Cell	8 (44%)	8 (42%)	0.77
Unspecified	2 (11%)	1 (5%)	
Stage at Diagnosis			
Stage I	6 (33%)	6 (32%)	
Stage II	1 (6%)	2 (11%)	0.96
Stage III	4 (22%)	4 (21%)	
Stage IV	7 (39%)	7 (37%)	
Years of HIV Infection	17 (2-36)		
HIV VL at Cancer Dx			
<400	6 (44%)		
>400	10 (56%)		
Median CD4	440 (26-872)		

Figure 1: Tissue Microarray of Cohort

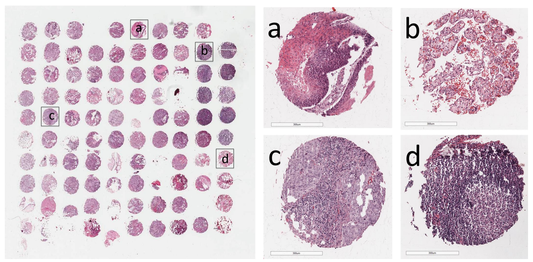
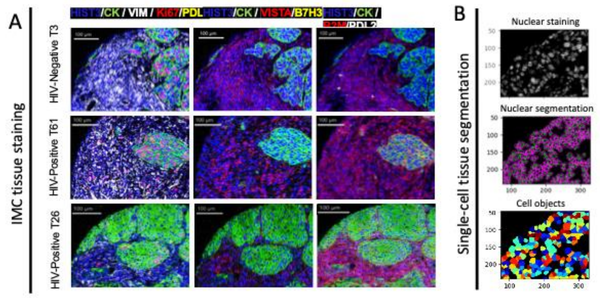
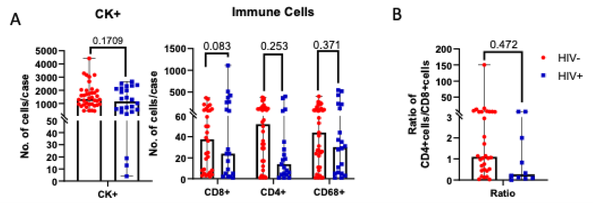


Figure 2: Immune Mass Cytometry



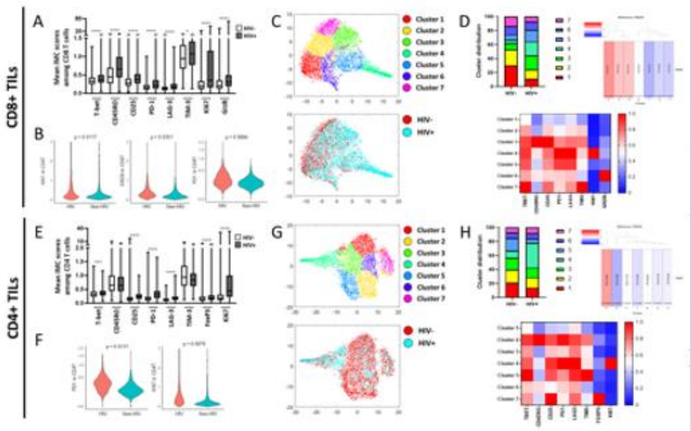
A) Representative multicolor microphotographs of a single NSCLC tumor stained with a 37-marker IMC panel. Captions of the same tumor displaying different markers as indicated in the color-code of each panel. Bar=100 um. B) Representative image showing the single cell segmentation of IMC tumor images using nuclear-cell markers and digital cell objects

Figure 3: Immune Cell Infiltration



(A) Mean number of CK+ tumor cells, CD8+, CD4+ tumor-infiltrating lymphocytes (TIL) and CD68+ tumor-associated macrophages (TAM) in non-HIV controls (red bars) and in HIV-associated NSCLCs (blue bars). Each bar depicts the mean±SEM and each dot represents an individual patient. (B) CD4/CD8+ TIL ratio among control non-HIV NSCLC cases (red bar) and HIV-associated NSCLC cases (blue bar). Each bar depicts the mean±SEM

Figure 4: T Cell Phenotypes in TME



(A, E) Mean expression value of single markers within CD8+ T cells (A) and CD4+ T cells (E) from immune mass cytometry panels. * for p<0.05; *** for p<0.001; **** for p<0.0001 using non-parametric Kruskal-Wallis test (B, F) Umbrella plots revealed markers with significant differences between PWH and PWOH among CD8+ T cells (B) and CD4+ T cells (F) using random effects model (C,G) Unsupervised clustering analysis revealing 7 unique clusters of CD8+ (C) and CD4+ (G) T cells as a t-SNE plot in the top figure and distribution of cells by HIV status in bottom panel with cells from PWH (blue) and PWOH (red). (D, H) Bar graphs representing distribution of each CD8 (D) and CD4 (H) T cell cluster among PWH and PWOH. Fold change graphs demonstrate the change in proportions for each subset in HIV-associated tumors from PWH compared to non-HIV tumors from PWOH. Heat map showing intensity of each marker across the different clusters, normalized from 0 to 1 with 1 being highest expression.

Figure 5: Increased mortality observed among PLWH and late stage NSCLC compared to HIV- cases

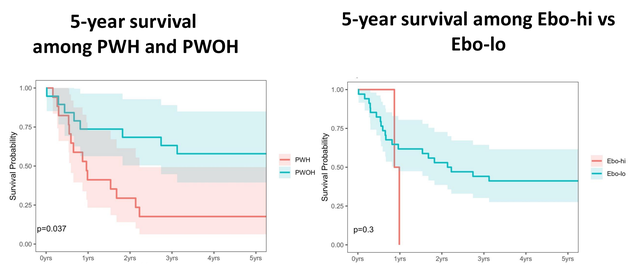
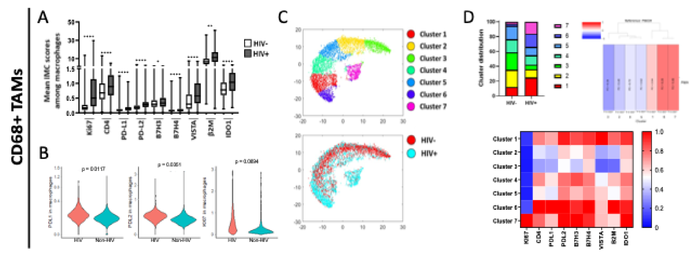
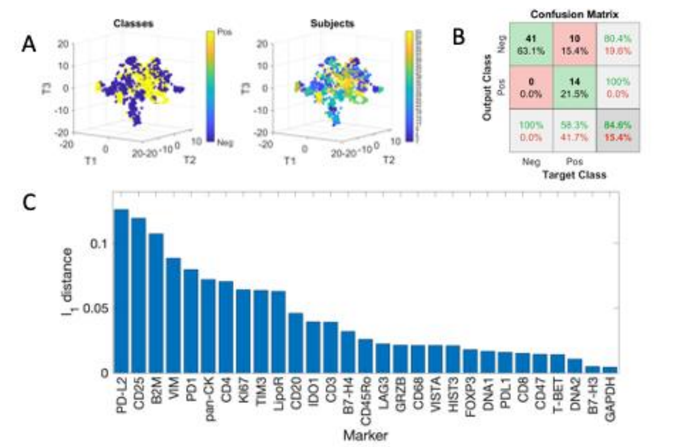


Figure 6: Tumor Associated Macrophages



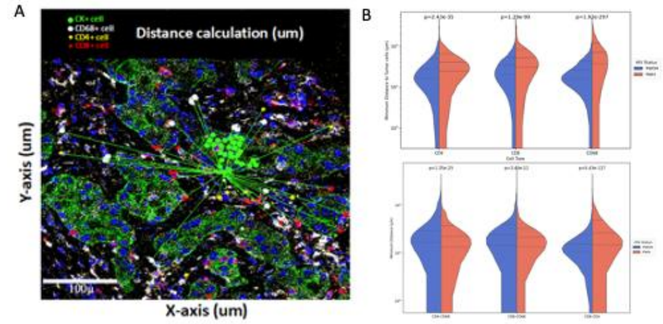
(A) Mean expression value of single markers within CD68+ tumor associated macrophages (TAMs) from immune mass cytometry panels. (B) Umbrella plots revealed markers with significant differences between PWH and PWOH among CD8+ T cells (B) and CD4+ T cells (F) using random effects model. (C) Unsupervised clustering analysis revealing 7 unique clusters of TAMs as a t-SNE plot in the top panel and distribution of cells by HIV status in bottom panel with cells from PWH (blue) and PWOH (red). (C) Bar graphs representing distribution of each TAM cluster among PWH and PWOH. Heat map showing intensity of each marker across the different clusters normalized from 0 to 1 with 1 being highest expression. Fold change graphs demonstrate the change in proportions for each subset in HIV-associated tumors from PWH compared to non-HIV tumors from PWOH.

Figure 7: Spectral Graph Theory Distinguishes HIV from non-HIV TME



(A) Visualization of patches representation in 3D using t-SNE, colored according to (left) the HIV status and (right) the subjects. (B) The confusion matrix for HIV prediction obtained using a leave-one-subject-out cross-validation based on a Radial Basis Function (RBF) Support Vector Machine (SVM)classifier. (C)Significance of antibodies ranked according to the L1 distance between their steady-state distributions (SSD) on the graph of 14 patches associated with the highest CK expressions.

Figure 7: Distance Between Immune Cell Subsets within TME



(A) Representative sample in which distances were calculated between individual cell populations (B) Distance (log-transformed) between pairs of cells from each of the three major immune cells subsets (CD4+ T cells, CD8+ T cells, and TAMs) to CK+ tumor cells (top panel) and between each of immune cell subsets (bottom panel). Index cell for each calculation is xyz. Wilcoxan rank test to test significance is noted (C)

Conclusion:

Our study demonstrates that the

- TME of PWH is characterized by a unique immune landscape with evidence of expansion of immune cells (T cells and macrophages) with enhanced immunoregulatory phenotypes
- T cells from PWH have associated impaired anti-tumor responses
- TME of NSCLC among PWH have altered spatial distribution of immune cells compared to PWOH, with immune cells having increased distances from tumor cells
- These findings have significant implications for response to immune checkpoint blocker therapies.

Acknowledgements